Energy spectra for a photonic analog of multilayer graphene

Wei Zhong[1] and Xiangdong Zhang[1,2,*]

[1]*Department of Physics, Beijing Normal University, Beijing 100875, China*

[2]*School of Physics, Beijing Institute of Technology, 100081, Beijing, China*

(Received 17 June 2011; revised manuscript received 27 July 2011; published 15 September 2011)

We present a multiple-scattering method to study the dispersion of multilayer honeycomb arrays of metallic nanoparticles. Three types of stacking are considered. It is shown that the energy spectra for these multilayer photonic structures strongly depend on the distances between the layers, stacking number of layers, and the type of stacking, which are closely analogous to the electronic ones in multilayer graphene. The effects of interlayer coupling on the energy spectra have been demonstrated by exact numerical simulations. Thus, extensive applications of such a phenomenon to design optical devices are anticipated.

DOI: 10.1103/PhysRevA.84.033826 PACS number(s): 42.70.Qs, 41.20.Jb, 73.20.Mf

I. INTRODUCTION

In recent years, there has been a great deal of interest in studying the physical properties of graphene due to the successful fabrication experiments of Novoselov *et al.* [1]. At the beginning, the investigations mainly focused on monocrystalline graphene consisting of carbon atoms densely packed in a honeycomb lattice, which can be viewed as either an individual atomic plane pulled out of bulk graphite or unrolled single-wall carbon nanotubes. Owing to its unique band structure, the electronic property of the monolayer graphene was found to be significantly different from the conventional two-dimensional (2D) structures [2,3]. Recently, the multilayer systems containing a few layers of graphene have also been fabricated as well [4–6]. There the interlayer coupling drastically changes the band structure, giving characteristic features depending on the number of layers [7–18]. Some unusual physical properties have been observed in these multilayer graphenes [4–18].

Analogous to these electron systems, the optical transmission near the Dirac point in 2D photonic crystals (PCs) has also been discussed [19,20]. In some 2D PCs with triangular or honeycomb lattices, the band gap may become vanishingly small at corners of the Brillouin zone, where two bands touch as a pair of cones. Such a conical singularity is also referred to as the Dirac point similar to the case of electron graphene. Many interesting phenomena in optics relevant to the photonic Dirac cone have been demonstrated [21–23]. Recently, another photonic analog of graphene, namely, a honeycomb array of metallic nanoparticles, has been proposed and analyzed theoretically [24]. Particle plasmon resonances in the nanoparticles act as localized orbitals in carbon atom. The tight-binding picture is thus reasonably adapted to this system, and nearly flat bands are found in the zigzag edge. However, all these investigations are for the photonic analog of monolayer graphene. The problem is whether or not the photonic analog of multilayer graphene can also be realized.

Motivated by such a problem, in this work we present a multiple-scattering method to study the dispersion of a multilayer honeycomb array of metallic nanoparticles. The energy spectra for three stacking types of structures are obtained. The numerical simulations are also performed. The rest of this paper is arranged as follows. In Sec. II, we introduce theory and method. The results and discussion are described in Sec. III. A conclusion is given in Sec. IV.

II. THEORY AND METHOD

We consider three stacking types of multilayer photonic structures as shown in Figs. 1(a)–1(c), respectively, in which each dot in the figures represents a metal sphere embedded in a homogeneous medium with the permittivity ε and the magnetic permeability μ. The metal spheres in each monolayer are arranged in a honeycomb lattice. The red (gray) dots represent the spheres in one unit cell. The number of the sphere in the unit cell (n) is twice as big as the number of the layer (N), namely $n = 2N$. The distance between adjacent spheres in every monolayer is $a_0 = a/\sqrt{3}$, where a is the lattice constant. The distance between adjacent layers is marked by d. We assume that the multilayer sample is infinite in x and y directions and of finite thickness in the z direction.

Since the system is periodic in the x and y directions, the problem can be reduced to a supercell calculation. The key point of the supercell method is to design an appropriate auxiliary infinite periodic superstructure in order to apply the Bloch theorem. The auxiliary superstructure is formed by the infinite periodic translation of the supercell along both x and y axes. If we assume that the relative location of the jth sphere in the supercell is $\vec{\delta}_j$ ($\vec{\delta}_j$ is the vector in three-dimensional space) and consider a plane electromagnetic wave of angular frequency ω with the electric field component $\vec{E}(r,t) = \mathrm{Re}[\vec{E}(r)\exp(-i\omega t)]$ incident on the system, the total scattered field can be given by using the Bloch theorem [25,26]:

$$\vec{E}_{sc}(\vec{r}) = \sum_{j=1}^{n}\sum_{l=1}^{\infty}\sum_{m=-l}^{l}\left[\frac{i}{q}b_{jlm}^{+E}\overrightarrow{\nabla}\times\sum_{\vec{R}_n}\exp(i\vec{k}\cdot\vec{R}_n)h_l^+(qr_{nj})\vec{X}_{lm}(\hat{r}_{nj}) + b_{jlm}^{+H}\sum_{\vec{R}_n}\exp(i\vec{k}\cdot\vec{R}_n)h_l^+(qr_{nj})\vec{X}_{lm}(\hat{r}_{nj})\right], \quad (1)$$

*zhangxd@bnu.edu.cn

 ©2011 American Physical Society

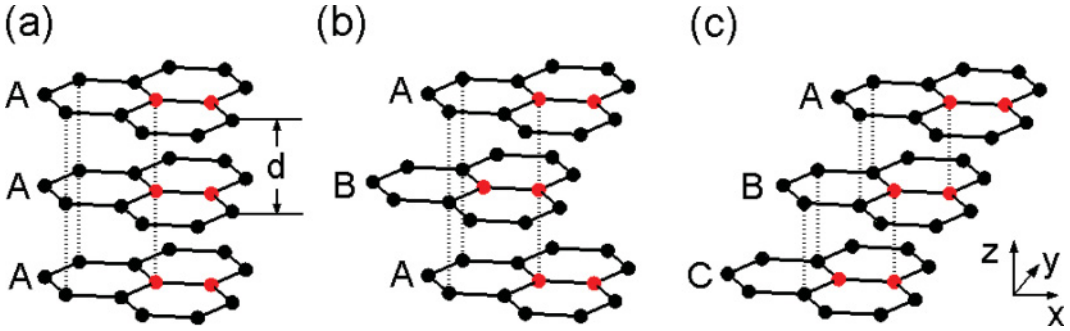

FIG. 1. (Color online) Three stacking structures of the multilayer photonic analog of graphene with (a) *AAA* stacking, (b) *ABA* (Bernal) stacking and (c) *ABC* (rhombohedral) stacking. The monolayer is the honeycomb lattice consisted of metal spheres. The red (gray) dots represent the metal spheres in one unit cell.

with a corresponding expression for $\vec{H}_{sc}(\vec{r})$ obtained according to the transformation $E \to H$, $H \to E$, and $\varepsilon \to -\mu$, and where $q = \sqrt{\varepsilon}\omega/c$ and $\vec{r}_{nj} = \vec{r} - (\vec{R}_n + \vec{\delta}_j)$, c is the velocity of light in vacuum, $\vec{k}$ is the Bloch vector, and $\vec{R}_n$ represents a two-dimensional (Bravais) lattice vector. h_l^+ are the spherical Hankel functions, $\vec{X}_{lm}$ are vector spherical harmonics; $b_{jlm}^{+P}(P = E, H)$ are the scattered coefficients of the jth sphere in the supercell, which are determined by the incident plane wave and the scattered wave from all the other spheres in the system. The wave scattered from all the other spheres can be expanded into a series of incident vector spherical waves around the j'th sphere as [25,26]

$$\vec{E}'_{j'sc}(\vec{r}) = \sum_{l=1}^{\infty}\sum_{m=-l}^{l}\left(\frac{i}{q}b'^{E}_{j'lm}\vec{\nabla}\times j_l(qr_{nj'})\vec{X}_{lm}(\hat{r}_{nj'}) + b'^{H}_{j'lm}j_l(qr_{nj'})\vec{X}_{lm}(\hat{r}_{nj'})\right), \quad (2)$$

and a corresponding expression for the magnetic field can also be obtained similarly. The b'^{P}_{jlm} coefficients in these expressions are to be determined by the following equation:

$$b'^{P}_{jlm} = \sum_{j'=1}^{n}\sum_{P'=E,H}\sum_{l'm'}\Omega^{PP'}_{jlm,j'l'm'}\,b^{+P'}_{j'l'm'}, \quad (3)$$

where $\Omega^{PP'}_{jlm,j'l'm'}$ is the free-space propagator, for which the explicit expression is given in the Appendix. The key to calculate the propagator of the system is the problem of lattice sum, namely "structure constants," also given in the Appendix. If the external incident field is expanded in vector spherical waves and the expansion coefficients are characterized by a^{0P}_{jlm} [25,26], we have the Rayleigh identities

$$b^{+P}_{jlm} = T^{P}_{jlm}\left(\sum_{j'=1}^{n}\sum_{P'=E,H}\sum_{l'm'}\Omega^{PP'}_{jlm,j'l'm'}b^{+P'}_{j'l'm'} + a^{0P}_{jlm}\right), \quad (4)$$

where T^{P}_{jlm} are the elements of the scattering matrix by the single isotropic sphere, which can be obtained analytically. This is the basic equation for the present multiple-scattering system. The normal modes of the system may be obtained by solving the following secular equation in the absence of an external incident wave:

$$\det\left|\delta_{PP'}\delta_{jj'}\delta_{ll'}\delta_{mm'} - \sum_{l''m''P''}\Omega^{PP'}_{jlm,j''l''m''}T^{P}_{jlm,j'l'm'}\right| = 0. \quad (5)$$

Here $T^{P}_{jlm,jl'm'} = T^{P}_{jlm}\delta_{ll'}\delta_{mm'}$ for an isotropic sphere. Based on such an equation, the energy spectra for the photonic analog of multilayer graphene can be obtained through the numerical calculations. In our method, we do not take a supercell in which slabs of multilayer alternate with slabs of vacuum as in Ref. [27]. Thus, some spurious unphysical solutions due to an unphysical assumption of periodical supercell can be avoided.

III. NUMERICAL RESULTS AND DISCUSSION

In this part we present the numerical results on the energy spectra for photonic analog of multilayer graphene. The permittivity of the metal sphere is described by the Drude type $\varepsilon(\omega) = 1 - \omega_p^2/\omega^2$ with $\omega_p = 6.18$ eV [24]. The radius of the sphere is 10 nm, and the lattice constant $a = 60$ nm. The calculated energy spectrum for the monolayer structure with these parameters is plotted in Fig. 2(a). The existence of a Dirac point at 3.9023 eV in such a monolayer energy spectrum has been demonstrated in Ref. [24]. However, with the introduction of another layer, the situation becomes different due to the coupling effect. The calculated results of the energy spectra of double layers for *AAA* stacking with interlayer distances $d = 2.0a$, $1.0a$, and $0.5a$ are plotted in Figs. 2(b)–2(d), respectively. When the distance between two layers is large, for example $d = 2.0a$, the coupling between two layers is weak and the energy spectra are basically in agreement with that of a monolayer [see Figs. 2(a) and 2(b)]. With the decrease of the interlayer distance, the coupling effect between two layers becomes strong and new phenomena appear. For example, as $d = 1.0a$, two cross points around the frequency of the Dirac point for the monolayer are observed [Fig. 2(c)], while the linear dispersion disappears completely and the feature of the conductance band appears as $d = 0.5a$ [see Fig. 2(d)].

In order to demonstrate this interlayer coupling effect, we perform a numerical simulation of the wave transport in the finite sample by using the multiple-scattering method with the incidence of a fundamental Gaussian beam. To simulate the transport of the fundamental Gaussian beam in nanoparticle structures by such a method has been described in Ref. [28]. Here, we take two-layer systems ($N = 2$) corresponding to the cases in Fig. 2, which have $20a$ length (y direction), $21a$ width

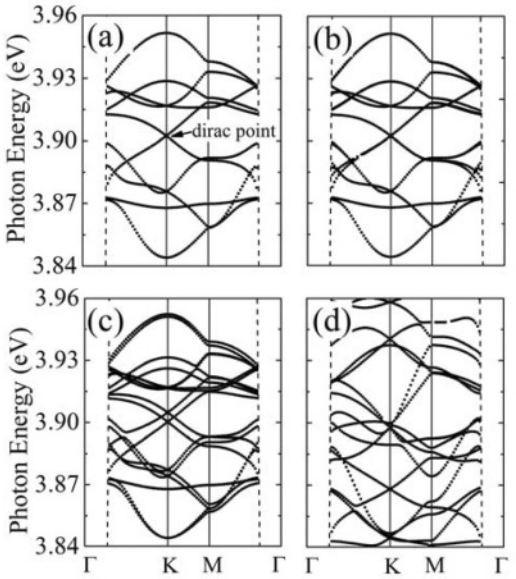

FIG. 2. (a) The dispersion relation of monolayer plasmonic spheres. There exists a Dirac point at 3.9023 eV; (b)–(d) the dispersion relations of bilayer plasmonic spheres ($N = 2$) with *AAA* stacking. The distance between the two monolayers is (b) $d = 2.0a$, (c) $d = 1a$, (d) $d = 0.5a$. The dashed lines in the figures indicate the light lines. The lattice constant is 60 nm, the sphere radius is 10 nm, and $\omega_p = 6.18$ eV.

(x direction) in each monolayer. We set the first monolayer at $z = 0$ plane and the second monolayer at $z = -d$ plane. The Gaussian beam propagating in the z direction with its electric field polarized along the y axis is focused at $(0, -7.5a, 0)$, namely, at the edge of the first monolayer. The numerical aperture (NA) of the Gaussian beam is taken as NA = 0.3, and the electric intensity $|E|$ at the center of the beam is normalized as 1. The frequency of the Gaussian beam is taken as 3.9023 eV corresponding to the Dirac point for the monolayer and the other parameters of the sample are also identical with those used in Fig. 2. Although the Gaussian beam propagates along the z direction, the propagating behavior of the wave can also be observed due to the coupling effect when the guide modes exist in the monolayer [28]. In contrast, the diffusion behavior should exhibit when the frequency locates at the Dirac point.

For comparison, in Fig. 3(a) we first plot the distribution of the electric field intensity for the monolayer structure (there is no second layer at $z = -d$ plane) when the center of the incident Gaussian beam with 3.9023 eV locates at the position marked by the red (gray) X in the figure. We find that the propagation of light inside the sample exhibits the resembling diffusion behavior. The calculated results of electric field intensity patterns inside the first monolayer ($z = 0$ plane) for the two-layer systems corresponding to Figs. 2(b)–2(d) are shown in Figs. 3(b)–3(d), respectively. It can be seen clearly that the distributions of field intensities strongly depend on the distance between two layers. When the distance between two layers is taken as $d = 2.0a$ or $1.0a$ [Fig. 3(b) or 3(c)], the field distributions change slightly. This is because the dispersion features of the structures are almost unchanged at such a frequency except for some shifts. However, for the case with $d = 0.5a$, the distribution of the field intensity as shown in Fig. 3(d) is quite different from those in Figs. 3(a)–3(c) due to the strong coupling effect between two layers. The propagating mode of the wave inside the layer is observed clearly in such a case, which also corresponds to the energy spectrum in Fig. 2(d).

In fact, the energy spectra not only depend on the distance between two layers, they are also related to the stacking number of layers. Figures 4(a) and 4(b) show the dispersion relation

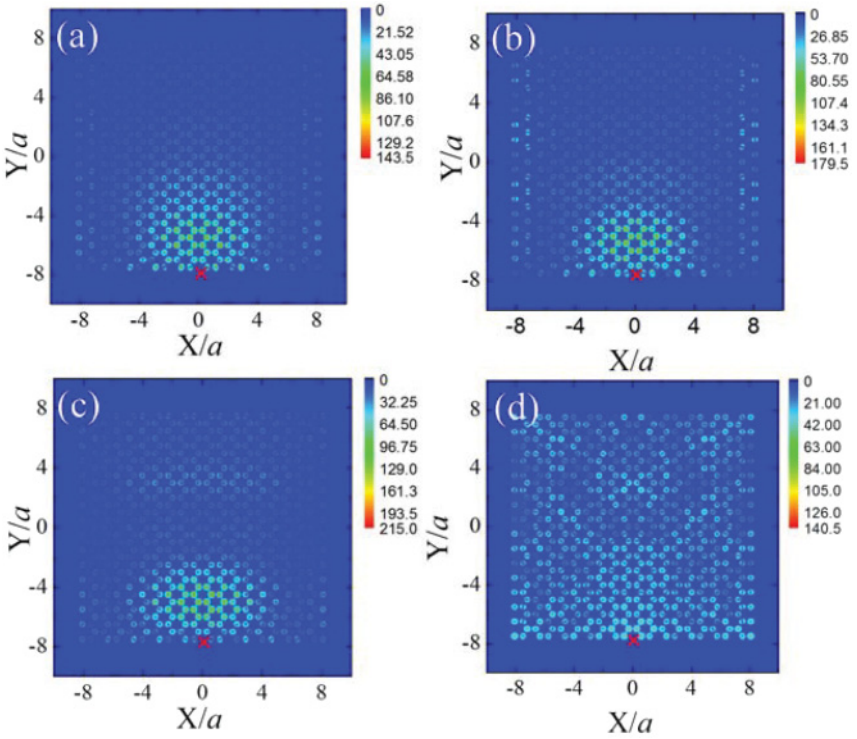

FIG. 3. (Color online) Distributions of the electric field intensity inside the first monolayer under the incidence of a fundamental Gaussian beam propagating along the z direction with numerical aperture NA = 0.3 at 3.9023 eV. The length (y direction) and width (x direction) of the sample are taken as $20a$ and $21a$, respectively. (a) Without the second monolayer; (b) the distance between the two monolayer is $d = 2.0a$; (c) $d = 1.0a$; (d) $d = 0.5a$. The other parameters are identical with those in Fig. 2. The red X is the center of the Gaussian beam.

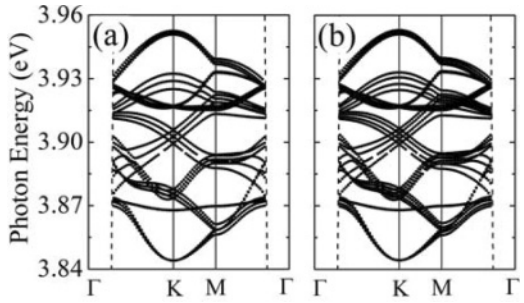

FIG. 4. The dispersion relations of the multilayer systems with *AAA* stacking. (a) $N = 3$, (b) $N = 4$. The dashed lines indicate the light lines. The distances between the adjacent monolayers are taken as $d = 1.0a$. The other parameters are identical with those in Fig. 2.

of three-layer and four-layer systems under the *AAA* stacking, respectively. Here the distances between adjacent layers are taken as $d = 1.0a$. The energy spectra with three and four cross points are observed clearly. Some cross points deviate from the *K* point because of the coupling effect among the layers.

The above results are only for the case of the *AAA* stacking. If we change the type of stacking, the energy spectra exhibit different features. For example, Figs. 5 and 6 display the calculated results of the energy spectra for the *ABA* and the *ABC* stacking with various layers, respectively. Figure 5(a) corresponds to the dispersion relation of the two-layer system with AB stacking, and Fig. 5(b) is its partial enlargement in the red square frame. Figures 5(c)–5(e) are the corresponding partial enlargement figures with $N = 3$, 4, and 5, respectively, while Fig. 6 represents partial enlargement figure for the cases under the *ABC* stacking. Comparing them, we find that some interesting phenomena for the electron multilayer graphene can also be observed in the present photonic structures. For example, the parabolic dispersion relations appear for the Bernal stacking, which are different from those in the *AAA* stacking structures. And linear dispersions only appear for the odd-layer system of the Bernal stacking [red (gray) lines in Figs. 5(c) and 5(e)]. A spontaneous gap at the *K* point can open for the *ABC* stacked trilayer [Fig. 6(a)], it disappears with the increase of the stacked number of layers. These features are closely analogous to the electronic ones in the multilayer graphenes. This means that we can construct photonic structures to control the transport of light similar to the multilayer graphene for electrons.

IV. CONCLUSION

In summary, three types of photonic graphene structures with *AAA*, bernal, and rhombohedral stacking have been designed by using metallic nanoparticles. The dispersion relations of these structures have been investigated by using a rigorous multiple-scattering method. The effects of distances between the layers, stacking numbers, and types of stacking on the energy spectra of the structures have been discussed. Some unusual phenomena in the energy spectra for the electron in multilayer graphenes have been observed for the photon in the present photonic graphene structures. This means that the transport properties of light similar to the case of electrons in multilayer graphene can be realized by constructing photonic nanostructures. That is to say, our findings provide a way to control the transport of light similar to the multilayer graphene for electrons and thereby open up the possibility for developing new nanophotonic devices.

ACKNOWLEDGMENTS

This work was supported by the National Natural Science Foundation of China (Grant No. 10825416) and the National Key Basic Research Special Foundation of China under Grant No. 2007CB613205.

APPENDIX

In this Appendix, we provide the explicit expressions for the free-space propagator ($\Omega^{PP'}_{jlm,j'l'm'}$) and "structure constants" by Ewald's treatment of lattice sums for the present slab system. The free-space propagator is expressed as [26]

$$\begin{aligned}\Omega^{EE}_{jlm;j'l'm'} &= \Omega^{HH}_{jlm;j'l'm'} \\ &= (\psi_l\psi_{l'})^{-1}\left[2\alpha_l^{-m}\alpha_{l'}^{-m'}Z_{j'l'm'-1;jlm-1}\right. \\ &\quad \left. + mm'Z_{j'l'm';jlm} + 2\alpha_l^{m}\alpha_{l'}^{m'}Z_{j'l'm'+1;jlm+1}\right],\end{aligned} \tag{A1}$$

$$\begin{aligned}\Omega^{HE}_{jlm;j'l'm'} &= -\Omega^{EH}_{jlm;j'l'm'}, \\ &= (2l+1)(\psi_l\psi_{l'})^{-1}\cdot\left[-2\alpha_{l'}^{-m'}\gamma_l^{m}Z_{j'l'm'-1;jl-1m-1}\right. \\ &\quad \left. + m'\zeta_l^{m}Z_{j'l'm';jl-1m} + 2\alpha_{l'}^{m'}\gamma_l^{-m}Z_{j'l'm'+1;jl-1m+1}\right]\end{aligned} \tag{A2}$$

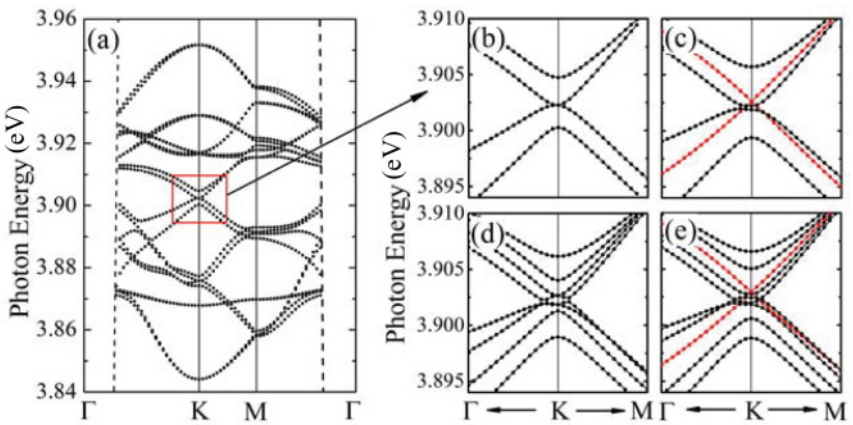

FIG. 5. (Color online) The band structures of the multilayer systems with the *ABA* (Bernal) stacking. (a) The dispersion for $N = 2$; (b) the *partial enlargement of the* dispersion in the red square frame shown in (a); (c) $N = 3$, (d) $N = 4$, (e) $N = 5$. The distances between the adjacent monolayers are taken as $d = 1.0a$. The other parameters are identical with those in Fig. 2.

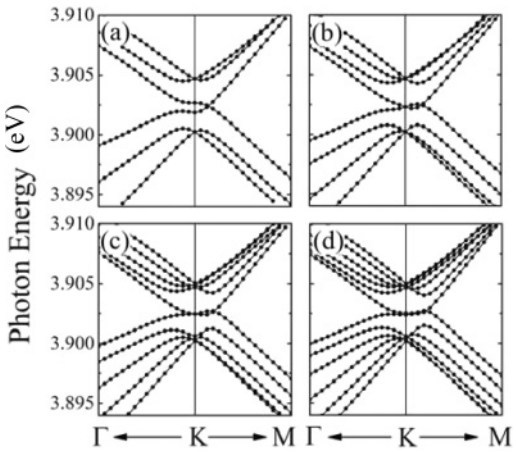

FIG. 6. The band structure (*partial enlargement*) of the multilayer systems with the *ABC* (rhombohedral) stacking. (a) $N = 3$, (b) $N = 4$, (c) $N = 5$, (d) $N = 6$. The other parameters are identical with those in Fig. 2.

with

$$\psi_l = \sqrt{l\,(l+1)}, \tag{A3}$$

$$\alpha_l^m = \frac{1}{2}\sqrt{(l-m)\,(l+m+1)}, \tag{A4}$$

$$\gamma_l^m = \frac{1}{2}[(l+m)\,(l+m-1)]^{1/2}/[(2l-1)\,(2l+1)]^{1/2}, \tag{A5}$$

$$\zeta_l^m = [(l+m)(l-m)]^{1/2}/[(2l-1)(2l+1)]^{1/2}, \tag{A6}$$

$$Z_{jlm,j'l'm'} = \sum_{\vec{R}_n}{}^{\dagger} g_{lm,l'm'}(\vec{\delta}_j - \vec{\delta}_{j'} - \vec{R}_n) e^{i\vec{k}\cdot\vec{R}_n}, \tag{A7}$$

$$g_{lm,l'm'}(\vec{r}) = \sum_{l''=0}^{\infty} \sum_{m''=-l''}^{l''} 4\pi(-1)^{(l-l'-l'')/2}(-1)^{m'+m''} h_{l''}^{(1)}(qr) \times Y_{l''-m''}(\hat{\Omega}(\vec{r})) \cdot \int Y_{lm}(\hat{\Omega}) Y_{l''m''}(\hat{\Omega}) Y_{l'-m'}(\hat{\Omega}) d\hat{\Omega}. \tag{A8}$$

In Eqs. (A7) and (A8), there is a problem of lattice sum, namely "structure constants,"

$$D_{lm} = \sum_{\vec{R}_n}{}^{\dagger} e^{i\vec{k}\cdot\vec{R}_n} h_l(q|\vec{\delta} - \vec{R}_n|) Y_{lm}(\hat{\Omega}(\vec{\delta} - \vec{R}_n)). \tag{A9}$$

The $\dagger$ means that $\vec{R}_n = \vec{0}$ should be omitted in the series when $\vec{\delta} = \vec{0}$. Here we use Ewald's methods to calculate the lattice sums. Ewald's methods are fairly standard in the solid state physics where they are used to evaluate structure constants in electron scattering theory [29,30]. The case of the 2D periodicity in a three-dimensional system has been treated by Kambe [31]. For the present system, the "structure constants" can be given by using Ewald's methods [31]:

$$D_{lm} = D_{lm}^{(1)} + D_{lm}^{(2)} + D_{lm}^{(3)}. \tag{A10}$$

Here

$$D_{lm}^{(1)} = \frac{1}{iq\,(-1)^{l-m}} \frac{1}{Aq^l} \frac{i^{m+1}}{2^l} [(2l+1)\,(l-|m|)!\,(l+|m|)!]^{\frac{1}{2}} \cdot \sum_{\vec{K}_n} e^{i(\vec{k}+\vec{K}_n)\cdot\vec{\delta}_{xy} - im\varphi_{\vec{k}+\vec{K}_n}} \cdot \sum_{n=0}^{l-|m|} \frac{1}{n!} (\Gamma_K)^{2n-1} \Delta_K^n \times \sum_{s=n}^{\min(2n,l-|m|)} \binom{n}{2n-s} \frac{\delta_z^{2n-s} (|\vec{k}+\vec{K}_n|)^{l-s}}{\left(\frac{l-|m|-s}{2}\right)! \left(\frac{l+|m|-s}{2}\right)!}, \tag{A11}$$

$$D_{lm}^{(2)} = -\frac{i}{q} \frac{1}{\sqrt{2\pi}} \sum_{\vec{R}_n}{}^{\dagger} e^{i\vec{k}\cdot\vec{R}_j} Y_{lm}(\hat{\Omega}(\vec{\delta} - \vec{R}_n)) \frac{|\vec{\delta} - \vec{R}_n|^l}{q^l} \times \int_{\frac{1}{\eta}}^{\infty} \xi^{l-\frac{1}{2}} e^{-\frac{1}{2}(|\vec{\delta}-\vec{R}_n|^2 \xi - \frac{q^2}{\xi})} d\xi, \tag{A12}$$

$$D_{lm}^{(3)} = \left[-\frac{1}{\sqrt{4\pi}} - \frac{i}{q\pi} \sum_{j=0}^{\infty} \left(\frac{1}{2\eta}\right)^{\frac{1}{2}} \frac{\left(\frac{q^2\eta}{2}\right)^j}{j!(2j-1)} \right] \delta_{l,0}\delta_{m,0}\delta_{\vec{\delta},0}, \tag{A13}$$

where A represents the area of the supercell in the x-y plane; $\Gamma_K = \sqrt{q^2 - |\vec{k}+\vec{K}_n|^2}$ and $\vec{\delta} = \vec{\delta}_{xy} + \delta_z\vec{z}$ is the relative position of the sphere in the supercell.

$$\Delta_K^n = \int_{e^{-\pi i}\frac{\Gamma_K^2}{2}\eta}^{\infty} \xi^{-\frac{1}{2}-n} e^{-\xi + \frac{\Gamma_K^2 \delta_z^2}{4\xi}} d\xi. \tag{A14}$$

From the expressions of Eqs. (A11) and (A12), we find that the value of D_{lm} seems to be dependent of the parameter η. In fact, the calculated results show that D_{lm} is independent of the value of η.

[1] K. S. Novoselov, A. K. Geim, S. V. Morozov, D. Jiang, Y. Zhang, S. V. Dubonos, I. V. Grigorieva, and A. A. Firsov, Science **306**, 666 (2004).

[2] C. W. J. Beenakker, Rev. Mod. Phys. **80**, 1337 (2008).

[3] A. H. Castro Neto, F. Guinea, N. M. R. Peres, K. S. Novoselov, and A. K. Geim, Rev. Mod. Phys. **81**, 109 (2009).

[4] K. S. Novoselov, E. McCann, S. V. Morozov, V. I. Fal'ko, M. I. Katsnelson, U. Zeitler, D. Jiang, F. Schedin, and A. K. Geim, Nat. Phys. **2**, 177 (2006).

[5] T. Ohta, A. Bostwick, T. Seyller, K. Horn, and E. Rotenberg, Science **313**, 951 (2006).

[6] T. Ohta, A. Bostwick, J. L. McChesney, T. Seyller, K. Horn, and E. Rotenberg, Phys. Rev. Lett. **98**, 206802 (2007).

[7] J. Nilsson, A. H. Castro Neto, F. Guinea, and N. M. R. Peres, Phys. Rev. Lett. **97**, 266801 (2006).

[8] B. Partoens and F. M. Peeters, Phys. Rev. B **75**, 193402 (2007).

[9] M. Koshino and T. Ando, Phys. Rev. B **76**, 085425 (2007); **77**, 115313 (2008).

[10] J. L. Mañes, F. Guinea, and M. A. H. Vozmediano, Phys. Rev. B **75**, 155424 (2007).
[11] P. Plochocka, C. Faugeras, M. Orlita, M. L. Sadowski, G. Martinez, and M. Potemski, Phys. Rev. Lett. **100**, 087401 (2008).
[12] J. Hass, F. Varchon, J. E. Millán-Otoya, M. Sprinkle, N. Sharma, W. A. de Heer, C. Berger, P. N. First, L. Magaud, and E. H. Conrad, Phys. Rev. Lett. **100**, 125504 (2008).
[13] M. Nakamura and L. Hirasawa, Phys. Rev. B **77**, 045429 (2008).
[14] M. Koshino and E. McCann, Phys. Rev. B **79**, 125443 (2009).
[15] A. A. Avetisyan, B. Partoens, and F. M. Peeters, Phys. Rev. B **79**, 035421 (2009); **80**, 195401 (2009).
[16] H. Min and A. H. MacDonald, Phys. Rev. Lett. **103**, 067402 (2009).
[17] M. Koshino and E. McCann, Phys. Rev. B **80**, 165409 (2009).
[18] E. V. Castro, M. P. López-Sancho, and M. A. H. Vozmediano, Phys. Rev. Lett. **104**, 036802 (2010).
[19] F. D. M. Haldane and S. Raghu, Phys. Rev. Lett. **100**, 013904 (2008); S. Raghu and F. D. M. Haldane, Phys. Rev. A **78**, 033834 (2008).
[20] R. A. Sepkhanov, Ya. B. Bazaliy, and C. W. J. Beenakker, Phys. Rev. A **75**, 063813 (2007); X. D. Zhang, Phys. Lett. A **372**, 3512 (2008).
[21] X. D. Zhang, Phys. Rev. Lett. **100**, 113903 (2008); X. D. Zhang and Z. Y. Liu, *ibid.* **101**, 264303 (2008).
[22] S. R. Zandbergen and M. J. A. de Dood, Phys. Rev. Lett. **104**, 043903 (2010).
[23] T. ochiai and M. Onoda, Phys. Rev. B **80**, 155103 (2009).
[24] D. Han, Y. Lai, J. Zi, Z.-Q. Zhang, and C. T. Chan, Phys. Rev. Lett. **102**, 123904 (2009).
[25] J. B. Pendry, *Low Energy Electron Diffraction* (Academic, London, 1974); N. Stefanou, V. Yannopapas, and A. Modinos, Comput. Phys. Commun. **113**, 49 (1998).
[26] A. Modinos, Physica A **141**, 575 (1987).
[27] R. D. Meade, K. D. Brommer, A. M. Rappe, and J. D. Joannopoulos, Phys. Rev. B **44**, R10961 (1991).
[28] J. Du, S. Liu, Z. Lin, J. Zi, and S. T. Chui, Phys. Rev. A **79**, 051801(R) (2009); A. A. R. Neves, A. Fontes, L. A. Padilha, E. Rodriguez, C. H. de Brito Cruz, L. C. Barbosa, and C. L. Cesar, Opt. Lett. **31**, 2477 (2006); X.-X. Liu and Andrea Alù, Phys. Rev. B **82**, 144305 (2010).
[29] P. Ewald, Ann. Phys. **64**, 253 (1921).
[30] F. S. Ham and B. Segall, Phys. Rev. **124**, 1786 (1961).
[31] K. Kambe, Z. Naturforsch. A: Phys. Sci. **22**, 422 (1967); **22**, 322 (1967); **23**, 1280 (1968).